Nanomedicine: Nanotechnology, Biology, and Medicine 58 (2024) 102751

Contents lists available at ScienceDirect

Nanomedicine: Nanotechnology, Biology, and Medicine

journal homepage: www.sciencedirect.com/journal/nanomedicine-nanotechnology-biology-and-medicine

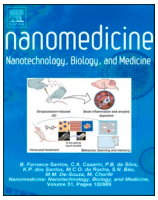

Original Article

Riboflavin-targeted polymers improve tolerance of paclitaxel while maintaining therapeutic efficacy

Milita Darguzyte, PhD [a,b,c,1], Elena Rama, MSc [a,1], Anne Rix, MSc [a], Jasmin Baier, MSc [a], Juliane Hermann, PhD [d], Sima Rezvantalab, PhD [e], Mohammad Khedri, MSc [f], Joachim Jankowski, PhD [d], Fabian Kiessling, MD [a,g,*]

[a] Institute for Experimental Molecular Imaging, University Hospital Aachen, Forckenbeckstrasse 55, 52074 Aachen, Germany
[b] University of Cologne, Faculty of Medicine and University Hospital Cologne, Department I of Internal Medicine, Center for Integrated Oncology Aachen Bonn Cologne Düsseldorf, Center for Molecular Medicine Cologne, 50931 Cologne, Germany
[c] Institute for Translational Immune-Oncology, Cancer Research Center Cologne-Essen (CCCE), University of Cologne, 50931 Cologne, Germany
[d] Institute of Molecular Cardiovascular Research, Medical Faculty, RWTH Aachen University, Aachen, Germany
[e] Department of Chemical Engineering, Urmia University of Technology, 57166-419, Urmia, Iran
[f] Computational Biology and Chemistry Group (CBCG) Universal Scientific Education and Research Network (USERN), 19839-63113 Tehran, Iran
[g] Fraunhofer MEVIS, Institute for Medical Image Computing, Forckenbeckstrasse 55, 52074 Aachen, Germany

ARTICLE INFO

Keywords:
Active targeting
Riboflavin
Paclitaxel
PEG
Molecular simulation
Drug delivery systems

ABSTRACT

Active targeting can enhance precision and efficacy of drug delivery systems (DDS) against cancers. Riboflavin (RF) is a promising ligand for active targeting due to its biocompatibility and high riboflavin-receptor expression in cancers. In this study, RF-targeted 4-arm polyethylene glycol (PEG) stars conjugated with Paclitaxel (PTX), named PEG PTX RF, were evaluated as a targeted DDS. In vitro, PEG PTX RF exhibited higher toxicity against tumor cells compared to the non-targeted counterpart (PEG PTX), while free PTX displayed the highest acute toxicity. In vivo, all treatments were similarly effective, but PEG PTX RF-treated tumors showed fewer proliferating cells, pointing to sustained therapy effects. Moreover, PTX-treated animals' body and liver weights were significantly reduced, whereas both remained stable in PEG PTX and PEG PTX RF-treated animals. Overall, our targeted and non-targeted DDS reduced PTX's adverse effects, with RF targeting promoted drug uptake in cancer cells for sustained therapeutic effect.

Background

Until now, chemotherapy has been indispensable for many cancer treatments, but its efficacy is often hampered by limited drug delivery to tumor sites and systemic side effects, primarily due to non-targeted distribution, multidrug resistance associated with a dense and complex tumor microenvironment, rapid drug clearance, and limited cellular uptake.[1,2] Nanomedicine has emerged to address these challenges. Drug solubility, stability, and bioavailability can be tailored by encapsulating chemotherapeutic agents within nanoparticles. Additionally, nanoparticles have shown increased drug accumulation in tumor tissues through the enhanced permeability and retention (EPR) effect, while minimizing exposure to healthy tissues, thus reducing systemic side effects.[3]

The EPR effect is a key mechanism that allows nanoparticles to selectively accumulate in tumor tissues with compromised vasculature. This effect is primarily observed in solid tumors and is attributed to abnormal and leaky tumor blood vessels, lack of lymphatic drainage, and the hypoxic tumor microenvironment.[4,5] Initially the EPR effect was presumed to be homogeneous and present in all tumor types, but its variability across patients and even within the same tumor has posed challenges for effective drug delivery and targeted treatments.[6,7] Indeed, despite significant advancements in nanomedicine formulations, their success in improving therapeutic outcomes and patient survival has been limited.[8,9]

To synergistically complement the EPR effect, several active targeting strategies have already been exploited showing enhanced drug retention in tumors and stronger cellular internalization, increasing

* Corresponding author at: Institute of Experimental Molecular Imaging, Forckenbeckstrasse 55, 52074 Aachen, Germany.
E-mail address: fkiessling@ukaachen.de (F. Kiessling).
[1] Both authors contributed equally

https://doi.org/10.1016/j.nano.2024.102751
Received in revised form 15 March 2024;
Available online 3 May 2024

their therapeutic performance.[10] Among the available tumor-targeting moieties, antibodies are the most efficient targeting systems. Due to their size, they offer an optimal balance between a long blood half-life, passive accumulation mediated by the EPR effect, and deep penetration, enabling efficient active targeting.[11] Thus, developing targeted nanomedicines in the size range of antibodies could leverage both passive accumulation and cellular internalization.

Vitamins have been studied as targeting moieties of nanomedicines in numerous clinical trials due to their biocompatibility, accessibility within the body, carrier properties, strong binding to specific receptors, and essential roles in cellular metabolism.[12,13] In this context, riboflavin (RF)-based targeting is emerging in oncology for diagnostic and therapeutic purposes. RF (Vitamin B2) is essential for cell proliferation and differentiation and, thus, required by metabolically active tissues, such as malignant tumors.[14] Even though the storing and transporting mechanisms are complex and only partially understood, it is mainly hypothesized that the riboflavin transporter 3 (RFVT3) is most responsible for RF uptake in tumors.[15] By exploiting this process, RF represents an optimal candidate to achieve higher therapeutic efficiency by actively triggering nanoparticle cellular internalization alongside passive tumor accumulation, avoiding drug release in the extracellular matrix (ECM), and the likelihood of side effects. As shown in previous studies conducted by our group, RF was successfully conjugated to a 3-arm peptostars and 4-arm polyethylene glycol (PEG)stars, strongly promoting its tumor cell internalization compared to the non-targeted counterpart. The benefit of RF-targeting in comparison to the unlabeled polymers' passive accumulation was demonstrated after Cy 5.5 labeling with computed tomography - fluorescence molecular tomography (CT/FMT), fluorescence microscopy, and ex vivo 2D fluorescence reflectance imaging (2D FRI).[16,17]

Despite these promising results, to the best of our knowledge, no prior study has elucidated whether the improved retention and internalization of RF-targeted compounds also result in more effective tumor therapy. Thus, in this study we conjugated 40 kDa star PEG with paclitaxel (PTX) (PEG PTX) and RF (PEG PTX RF) and investigated in vitro, in vivo, and ex vivo its therapeutic efficacy, looking at both, tumor response and drug tolerability.

Methods

Further details regarding Chemicals, Polymer characterization (including NMR analysis of Paclitaxel and Riboflavin derivatives, characterization of Targeted and non-targeted 4-arm PEGs, HPLC analysis, Dynamic light scattering, Nanoparticle tracking analysis, Fluorescence measurements, and Riboflavin targeted PEG interaction with riboflavin binding protein), Molecular dynamics simulation, In vitro cytotoxicity experiments, Animal housing, and Histology are provided in the Supplementary Information.

Synthesis

Paclitaxel (PTX) was conjugated to 4-arm polyethylene glycol (PEG) via a succinic spacer that releases the drug at physiological pH,[29] while riboflavin (RF) was coupled via carbodiimide linkage. Both PTX and RF needed functionalization before they could be linked to PEG. NMR was carried out at each step (supplementary information).

Paclitaxel derivative

PTX was functionalized to 2′-succinyl-paclitaxel (SPTX) according to.[29,30] Typically, 10 mg of PTX (1 eq.) were dissolved in pyridine and 14 mg of succinic anhydride (12 eq.) was added. The reaction was mixed overnight. Subsequently, the solvent was evaporated, and the residue was suspended in water. After 30 min of mixing, the solution was centrifuged, and the precipitate was collected. The precipitate was dried using a lyophilizer, and SPTX was obtained.

Riboflavin derivative

Carboxymethylriboflavin was synthesized according to.[31] RF was dissolved in 20 mL glacial acetic acid and 20 mL acetic anhydride. A few drops of perchloric acid (70–72 %) were added, and the mixture was stirred at 40 °C for 1 h. After cooling down, 40 mL of cold water was added, and the product was extracted with chloroform. Then, the solvent was removed under reduced pressure, and 2′,3′,4′,5′-tetra-*O*-acetylriboflavin was obtained.

Then, 2′,3′,4′,5′-tetra-*O*-acetylriboflavin (1 eq.) was reacted with ethyl bromoacetate (5 eq.) and anhydrous potassium carbonate (5 eq.) in anhydrous acetone. The mixture was stirred overnight at room temperature. Afterward, the solvent was removed under reduced pressure, and the product was dissolved in dichloromethane. The solution was washed with 1 N acetic acid and water. Then, the solvent was removed under reduced pressure, and N3-ethylacetate-2′,3′,4′,5′-tetra-*O*-acetylriboflavin was obtained.

To deprotect carboxy- and hydroxyl-groups, N3-ethylacetate-2′,3′,4′,5′-tetra-*O*-acetylriboflavin was refluxed in 2 M hydrochloric acid for 2 h. The solvent was removed under reduced pressure, and carboxymethylriboflavin was obtained.

Targeted and non-targeted 4-arm PEGs

PTX was conjugated to 4-arm PEG and then, in the case of targeted polymers (PEG PTX RF), RF was coupled. In detail, SPTX (1 eq.) was dissolved in dimethylformamide with N-(3-Dimethylaminopropyl)-N′-ethylcarbodiimide hydrochloride (1 eq.) and 1-Hydroxy-1H-benzotriazol Hydrate (1 eq.). After stirring for one day, PEG (4 eq.) was added, and the mixture was left to react for 18 h. The product was purified using HPLC.

For doubled labeled PEGs, further conjugation with carboxymethylriboflavin was performed. Carboxymethyl RF (4 eq.) was dissolved in dimethylformamide with 2-(1H-benzotriazol-1-yl)-1,1,3,3-tetramethyluronium hexafluorophosphate (4 eq.) and 1-hydroxy-1H-benzotriazol hydrate (4 eq.). After stirring for 1 h, purified SPTX-PEG (1 eq.) was added, and the mixture was left to react for 18 h. The product was purified using HPLC.

In vivo experiments

Tumors were induced by subcutaneous injection of 4×10^6 A431 cells in the right flank of ten-week-old Balb/c female nude mice (Crl: CD1-Foxn1nu, Janvier, France). Each day the animals were scored, and the tumor volume was measured using a caliper. Once the tumors reached 5 mm in diameter, the experiments started. Based on a previous study, the minimal effective dosage (MED) of our drug delivery systems was estimated to be between 5 and 20 nmol in 100 μL saline.[16] The timeline of the animal experiment was designed taking into consideration the rapid growth rate of untreated tumors (Control group) and the fast RF uptake. Indeed, Tsvetkova et al. observed a blood half-life of circa 13 h for RF targeted DDS.[16] In detail, the mice received 5 mg of PTX kg of body weight-1, normalized for all the therapies (free PTX, PEG PTX RF, or PEG PTX), or sodium chloride (control group) via intravenous injection on days 0, 2, and 4. Tumor response to therapy was monitored using contrast-enhanced ultrasound (Vevo3100, MX250 transducer, VisualSonics, Canada) using microbubbles (SonoMAC-r, SonoMAC GmbH, Germany) on days 0 (before therapy), 1, 3, 5, and 7. In detail, a series of images of tumors were acquired in B-Mode for tumor volume evaluation. Then, the transducer was positioned in the middle of the tumor, and the inflow of 1×10^7 microbubbles mL^{-1}, injected via tail vein, was acquired in non-linear contrast mode at a frequency of 18 MHz with a framerate of 10 fps for 90 s. Ultrasound images were analyzed using VevoLAB 3.2.0 to determine tumor volume, perfusion, and vascularization. On the last day, all animals were euthanized via cervical dislocation. Tumors and organs of interest were collected,

weighted, and preserved in Tissue-Tek (Sakura, Germany) at −80 °C.

Mass spectrometric data analysis

Sections of frozen mice livers, tumors, lungs, spleens, and kidneys were coated with a trypsin solution (25 ng/μL in 20 mM ammonium bicarbonate), incubated for 2 h at 50 °C and coated with α-cyano-4-hydroxycinnamic acid (Bruker Daltonic, Germany) as a matrix (10 mg/ml dissolved in 70 % ACN/ 0.2 % TFA). The coating process was performed using a MALDI imaging sprayer (HTX TM-Sprayer: TMSP-M3, HTX Technologies, USA). MALDI MSI data were accumulated using a TOF-TOF-mass spectrometer (Rapiflex; Bruker-Daltonic, Bremen, Germany) equipped with a SmartbeamTM 3D laser with a 5 kHz repetition rate and controlled by the Flex-Control 4.0 (Bruker-Daltonic, Germany). Mass spectra were acquired with 800 laser shots for each raster point and a digitizer rate of 2.5 GS/s in reflector-positive mode. Analyses were taken in the mass range of 0–3500 Da using a raster width of 50 μm.

Data analysis was performed using SCiLS Lab software (SCiLS Lab-2022b; SCiLS GmbH; Bremen, Germany) and Flex-Analysis 4.0 (Bruker-Daltonic, Bremen, Germany). MALDI MSI raw data sets were converted to the SCiLS SL file format. The baseline was calculated by an iterative top hat, and normalization was performed based on the total ion count (TIC) method. Peptides were identified through the MS/MS spectra using the lift option of the Rapiflex mass spectrometer (Bruker-Daltonic, Bremen, Germany). The mass spectra were calibrated and annotated using BioTools 3.2 (Bruker-Daltonic, Bremen, Germany) in combination with SwissProt (University of Geneva, Switzerland) and the MASCOT 2.2 database (Matrix Science, London, UK) comparing experimental mass-spectrometric data with calculated peptide masses for each entry into the sequence database.

Statistical analysis

Data were analyzed and visualized with GraphPad Prism V9.5 (GraphPad Software, La Jolla, CA, USA). One-way or two-way ANOVA test was performed to compare between control and other groups.

Results

Polymer conjugate synthesis and characterization

PTX conjugation to PEG stars (PEG PTX) was analyzed using high-performance liquid chromatography (HPLC), where the PTX peak was observed at 227 nm wavelength. Free PTX was found at a retention time (RT) of 24 min, while the PTX polymer conjugate (PEG PTX) displayed a peak at RT = 27 min indicating successful coupling. In NMR, a signal between 2.50 and 2.80 ppm was displayed corresponding to the succinic anhydride linkage of PEG PTX. The presence of the linker further confirmed the successful coupling of PTX.

Some PEG PTX was further functionalized with RF, obtaining PEG PTX RF. The presence of RF was affirmed by visual inspection (orange color) and by HPLC, where it was localized at 450 nm wavelength. At this wavelength neither PEG nor PTX are known to give any signal. Free RF displayed a peak at RT = 13 min, while the PEG PTX RF had a peak only at RT = 27 min.

The PEG PTX and PEG PTX RF sizes were analyzed using dynamic light scattering (DLS) (Fig. 1 A). PEG stars showed a bimodal distribution with sizes of 16 and 164 nm for non-targeted PEG PTX and 12 and 122 nm for targeted PEG PTX RF. Based on this, we assume that the polymers formed unimers and larger supramolecular structures. A few studies have reported that DLS measurements of samples having particles of two sizes (e.g., 20 and 100 nm) depending on the ratios of the particles could produce inaccurate results (e.g., have the results skewed towards the larger size).[18,19] Hence, multi-angle DLS was employed to get more accurate size measurements and additional information about the geometry. As shown in Fig. 1 B, the sizes of PEG stars did not change depending on the angle, where all polymer conjugates (PEG PTX and PEG PTX RF) had a radius of around 100 nm. Some smaller structures were seen only at a few angles, but the intensity of them compared to larger ones was so low that they were neglected (Fig. S1). Moreover, the Guinier plot was used to calculate the radius of gyration. The ratio of the radius of gyration and hydrodynamic radius of PEG PTX and PEG PTX RF was 1.5. Generally, the ratio of 1 suggests vesicle geometry, while the ratio of 1.5 is typical for multi-arm star-like polymers. Additionally, to check how samples behave at lower concentrations, nanoparticle tracking analysis (NTA) evaluation was performed (Fig. 1 C). NTA indicated a narrow uniform distribution with mode diameters of 166 ± 5 nm for PEG PTX and 128 ± 4 nm for PEG PTX RF, supporting and validating the previous DLS data.

Molecular dynamic simulations

In the simulation box, 12 simulated polymers (SPEG) were placed and allowed to interact for 100 ns. As can be seen from snapshots (Fig. 2 A-B), SPEG PTX and SPEG PTX RF assembled and formed supramolecular structures at the end of the simulation. In both cases, PTX molecules (depicted in red) were in the core of the formed structures. It is assumed that the vesicular formation is due to the hydrophobicity of the drug. SPEG PTX RF seems to form more compact structures (Fig. 2 B). Similar results were obtained when comparing the reduction of solvent-accessible surface area (SASA) from the initial to the final steps (Fig. 2 C). The SASA reduction was 34.23 % and 18.67 % for SPEG PTX RF and SPEG PTX, respectively, indicating increased aggregation in the presence of RF, which is believed to be due to hydrophobicity of RF. This was additionally confirmed by the radius of gyration (Rg) (Fig. 2 D). SPEG PTX RF and SPEG PTX showed polymer chains coming together to form

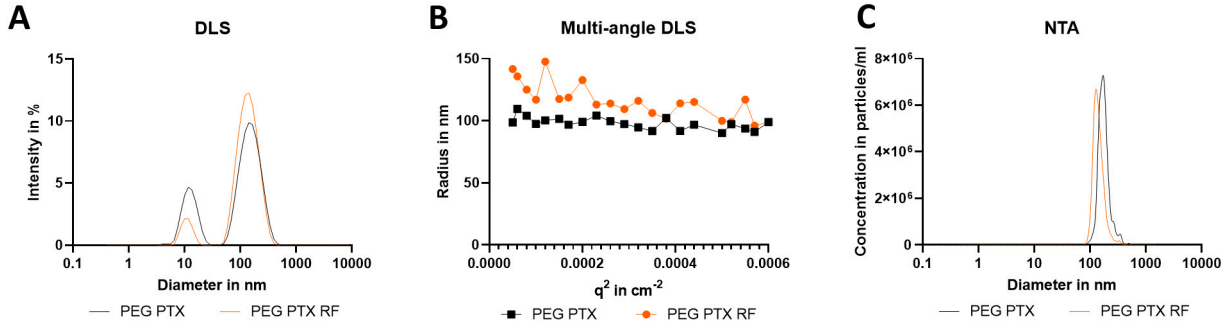

Fig. 1. Size measurements of PEG PTX RF and PEG PTX 4-arm PEGs. DLS measurements of PEG stars (A) show a bimodal distribution with larger particles having hydrodynamic diameters of 160 and 120 nm for concentrated PEG PTX and PEG PTX RF, respectively. Interestingly, multi-angle DLS measurements (B) do not display any significant differences between the polymers concerning the size or the uniformity of the samples. Both PEG stars seem monodispersed and have a radius of ~100 nm. NTA measurements (C) demonstrate narrow size distribution with mode diameters of 166 ± 5 and 128 ± 4 nm for PEG PTX and PEG PTX RF, respectively.

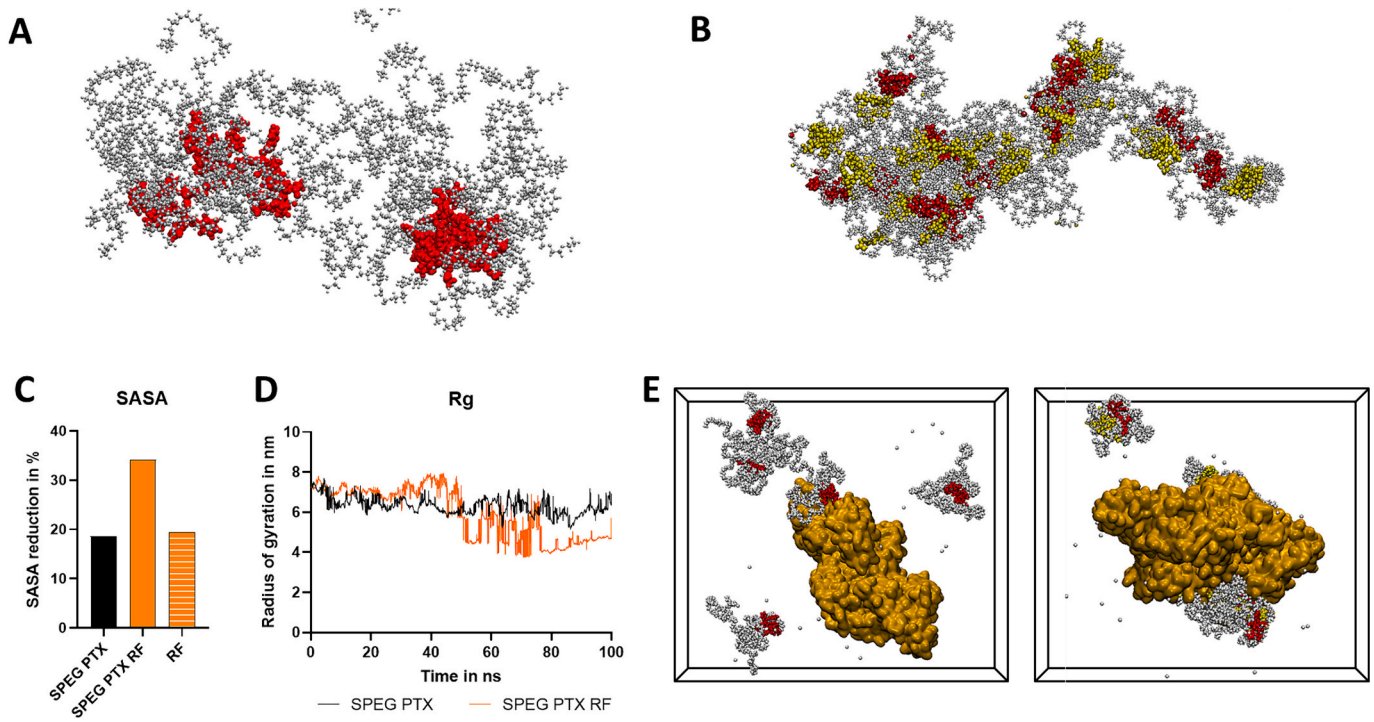

Fig. 2. Molecular simulation results. Snapshots of SPEG PTX (A) and RF SPEG PTX (B) molecular structures of polymers at the end of the simulation. RF is depicted in yellow, PTX in red, and SPEG chains in grey. RF SPEG PTX seems to be more compact than SPEG PTX. Solvent-accessible surface area (SASA) reduction (C) at the end of the simulation. SASA values are reduced for the RF SPEG PTX than the SPEG PTX ones indicating a higher degree of freedom in the latter. Similarly, the radius of gyration (Rg) (D) is lower in RF SPEG PTX than the SPEG PTX ones. (E) Snapshot of the simulation box at the end of simulation depicting interactions between simulated polymers (left: SPEG PTX, right: SPEG PTX RF) and bovine serum albumin (BSA).

more compact structures, with lower Rg observed for SPEG PTX RF. Overall, simulation results point to supramolecular structure formation, particularly in the presence of RF.

To simulate how the polymer chains behave in vivo, we also exposed five molecules of SPEGs to one molecule of bovine serum albumin (BSA) in the simulation box. In the presence of BSA, the polymers tended to come together (Fig. 2E). SPEG PTX RF also interacted with BSA, while most SPEG PTX molecules appeared distant from the BSA molecule.

In vitro RF binding and cytotoxicity

As PEG stars tend to form supramolecular structures, it is important to know whether RF structures can still interact with its receptors in tumor cell membranes. RF is known to be fluorescent (Fig. S2). Upon interacting with the riboflavin binding protein (RBP) it loses the fluorescence (Fig. 3 A). The reduction in fluorescence was observed when PEG PTX RF was exposed to increasing RBP amounts (Fig. 3 B). This confirmed that RF was not buried inside the supramolecular structures but stayed outside interacting with RBP or RFVT.

PEG polymers and RF are used in many products of our daily life and considered non-toxic.[20] To confirm the biocompatibility of their combination, human epidermoid carcinoma cells (A431) and prostate cancer (PC3) were used for cytotoxicity assays and exposed to high concentrations of RF-targeted polymers without PTX conjugation (PEG RF) and PEG, used as an additional control, for 24, 48, and 72 h (Fig. S3). As expected, the viability of the cells was not altered.

The cancer cell lines A431 and PC3 are known to overexpress human riboflavin transporters (RFVTs)[15,21] and were shown specifically to internalize RF polymers.[16] Hence, A431 (Fig. 4) and PC3 (Fig. S4) were exposed to a range of concentrations of free PTX, PEG PTX, and PEG PTX RF, respectively. Both PEG PTX and PEG PTX RF inhibited cell growth. With increasing exposure time, the inhibition efficacy increased for all probes. The free drug possessed the highest potency followed by PEG PTX RF, and PEG PTX. After 72 h exposure time, PEG PTX RF and PEG PTX had IC50 values of 0.0080 and 0.0129 nM in A431 cells, respectively (Fig. 5).

To further confirm the specificity of PEG PTX RF, vascular smooth muscle cells (vSMC), which are known not to overexpress RFVTs, were

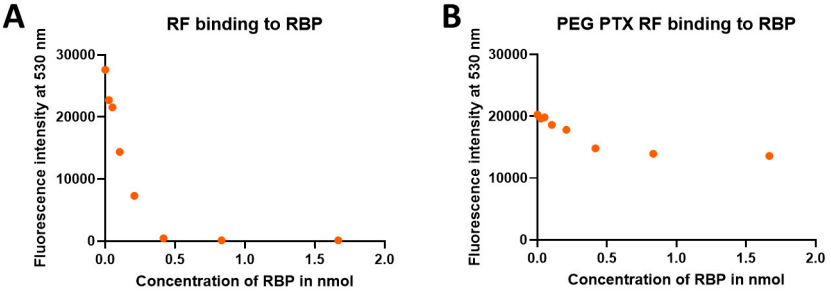

Fig. 3. Selective binding of free RF and PEG PTX RF to riboflavin binding protein (RBP). Fluorescence intensity plot (A) depicting decreasing fluorescence upon the interaction of free RF with RBP. The same result, though to a lesser extent, is found when exposing PEG PTX RF to RBP (B).

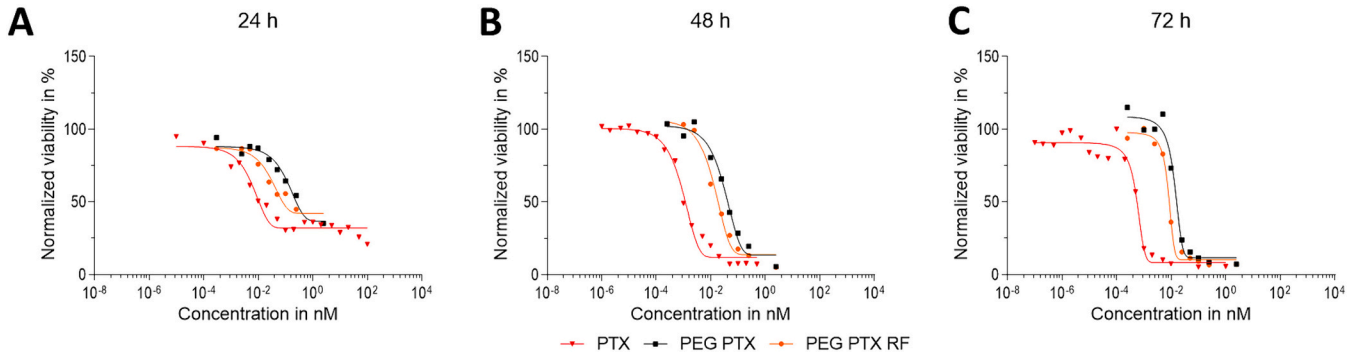

Fig. 4. Viability of A431 exposed to free PTX, PEG PTX, and PEG PTX RF polymers for 24, 48 and 72 h. Free PTX is depicted in red, PEG PTX in black, and PEG PTX RF in orange In all cases, the polymers (PEG PTX and PEG PTX RF) and the free drug inhibits cell growth. Expectedly, free PTX is most potent. RF targeting improves the cytotoxicity of PEG-PTX.

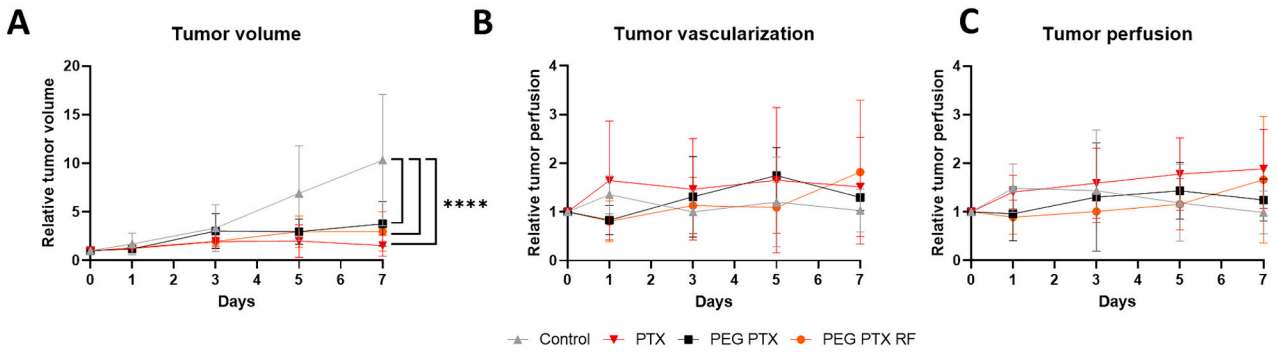

Fig. 5. Comparison of the antitumor effects of free PTX, PEG PTX, and PEG PTX RF. In comparison to untreated tumors (Control), tumor growth is significantly inhibited in animals receiving free PTX, PEG PTX and PEG PTX RF (A). No difference in tumor vascularization (B) and perfusion (C) is observed among the different groups. ****: $p \leq 0.0001$.

exposed to PEG PTX RF and compared to PEG PTX. While both RF PEG PTX and PEG PTX inhibited cell growth, as illustrated in Fig. S5, no discernible impact of RF targeting was observed. This observation is supported by the lack of a significant difference between the targeted and non-targeted DDS. Thus, no specific RF targeting was evident in the absence of RFVTs.

In vivo therapeutic efficacy

Animals with A431 xenograft tumors of 5 mm size were randomly allocated to one of the treatment groups, which were intravenously injected with sodium chloride (control group), free PTX, PEG PTX, or PEG PTX RF on days 0, 2, and 4, respectively. Tumor volume, perfusion, and vascularization were longitudinally evaluated via a contrast-enhanced ultrasound system (Vevo3100, VisualSonics, Canada) one day prior to the beginning of the therapy and on days 1, 3, 5, and 7. In comparison to untreated controls, free PTX and both PEG PTX formulations decreased the tumor volumes significantly (Fig. S6). No significant difference was observed in terms of tumor vascularization (Day 7 Control: 1.03 ± 0.39 a.u.; free PTX: 1.52 ± 0.95 a.u.; PEG PTX: 1.30 ± 0.24 a.u.; PEG PTX RF: 1.82 ± 1.32 a.u.) and perfusion (Day 7 Control: 0.98 ± 0.41 a.u.; free PTX: 1.88 ± 0.73 a.u.; PEG PTX: 1.24 ± 0.39 a.u.; PEG PTX RF: 1.66 ± 1.16 a.u.) among all the groups.

Ex vivo analysis

Ex vivo histological analyses were performed to further investigate the therapies' impact on tumor vascularization and proliferation. Hematoxylin and eosin (H&E) stains showed no difference in terms of necrosis among the four groups (Control: 15.27 ± 13.23 %; free PTX: 29.10 ± 11.54 %; PEG PTX: 21.47 ± 14.60 %; PEG PTX RF: 24.16 ± 15.96 %) (Fig. 6 A). Tumor vasculature was investigated via CD31 staining, revealing no changes in the amount of CD31 positive vessels among the treated groups and the untreated control (Control: 2.88 ± 0.78 %; free PTX: 4.07 ± 3.42 %; PEG PTX: 3.48 ± 1.38 %; PEG PTX RF: 3.78 ± 1.58 %) (Fig. 6 B). These findings are consistent with the in vivo ultrasound investigations.

Interestingly, although not statistically significant, cellular proliferation was most strongly inhibited by PEG PTX RF (28.27 ± 20.41 %), followed by PEG PTX (34.63 ± 18.52 %) and free PTX (41.99 ± 12.33 %). The percentage of proliferating cells in control tumors was 60.32 ± 29.54 % (Fig. 6 C).

Side effects of therapy

To assess the overall animal welfare, the body weight was measured daily. Animals receiving free PTX significantly lost body weight (93.33 ± 2.05 % of initial weight), while the weight of animals treated with PEG PTX and PEG PTX RF remained constant (at day 7 Control: 100.71 ± 3.07 %; PEG PTX: 106,52 ± 4.92 %; PEG PTX RF: 102,66 ± 2.86 %) (Fig. 7 A). At the end of the in vivo experiment, the animals were sacrificed. Organs, such as kidneys, spleen, liver, heart, and lungs were harvested and weighed (Fig. 7 B). A significant reduction in liver weights was observed in the free PTX group compared to untreated controls (at day 7: free PTX: 1.22 ± 0.13 g; Control: 1.46 ± 0.13 g). Interestingly, PEG PTX RF and PEG PTX did not significantly affect any organ weight. This highlights that the known liver toxicity of free PTX[22,23] can partially be compensated by our drug delivery system approach.

To further investigate the degree of liver toxicity for the different

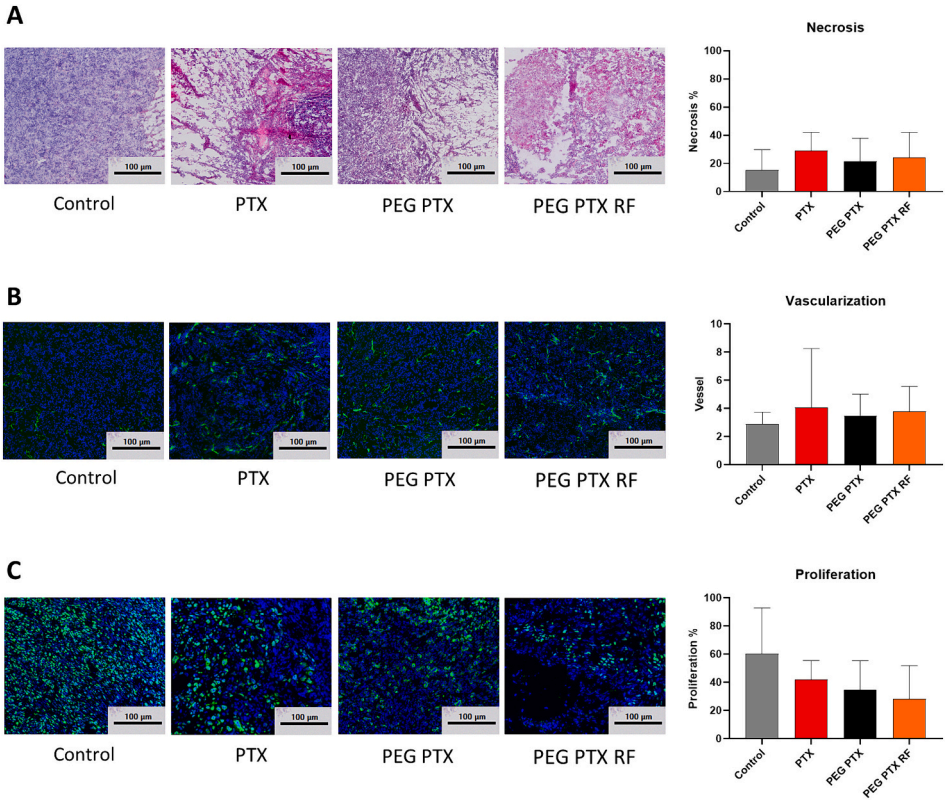

Fig. 6. Histological analysis of excised tumors. Representative images are shown on the left and the according quantification on the right. Quantification of necrosis (A) is based on H&E stainings (extracellular matrix depicted in pink and nuclei counterstained in purple); Functional vascularization (B) is assessed via CD31 staining in green. DAPI is used to counterstain the nuclei in blue; Proliferating cells (C) are visualized using a KI67 staining (green) and nuclei are displayed in blue (DAPI). No significant differences are found between the groups concerning the degree of necrosis and vascularization. However, inhibition of cells proliferation is observed for all the groups in comparison to the untreated control. This inhibitory effect is most pronounced for PEG PTX RF.

therapies (free PTX, PEG PTX, and PEG PTX RF), liver samples were analyzed by mass spectrometry (MS). Fresh frozen liver sections were trypsinized, enzymatically digested, and coated with a matrix to allow Matrix Assisted Laser Desorption/Ionization-Time of Flight (MALDI-TOF) analysis. The mass spectra were calibrated and compared with known peptide masses.

Major cell cycle factors were investigated. A higher expression of the cyclin-dependent kinase inhibitor 2A and 2B (CDN2A and CDN2B) was observed in the free PTX treated group in comparison to PEG PTX and PEG PTX RF groups (CDN2A Free PTX: 5.30e-^{05} ± 5.21 a.u.; PEG PTX: 2.26e^{-05} ± 1.94 a.u.; PEG PTX RF: 2.64e^{-05} ± 2.84 a.u.; CDN2B Free PTX: 1.65e-^{05} ± 0.74 a.u.; PEG PTX: 7.58e^{-06} ± 4.27 a.u.; PEG PTX RF: 8.23e^{-06} ± 7.35 a.u.) (Fig. 7 C—D).

Additional MALDI MSI was performed to investigate the amount of free PTX in spleen, lung, tumor, kidney and liver. While in most tissues almost no PTX metabolites were seen (Fig. S7), the liver had relatively high amounts (Fig. 7 D)·In particular, the free PTX treated group showed highest values of PTX accumulation in the liver, while it was reduced in PEG PTX and PEG PTX RF, indicating lower systemic toxicity for our polymeric drug delivery systems (Free PTX: 1.56*10^{-5} a.u.; PEG PTX: 2.84*10^{-6} a.u.; PEG PTX RF: 6.12*10^{-6} a.u.).

Discussion

Various drug delivery systems (DDS) have been developed to improve the efficacy and safety of chemotherapeutic drugs. DDS enhance passive drug accumulation via the EPR effect and decrease drug efflux from cancer cells.[4] They are also taken up by macrophages, which then slowly release the drugs to the cancer cells.[24]

To further improve retention and to increase the internalization by cancer cells, active targeting has been proposed.[25] However, to take benefit from active targeting DDS still need to reach the tumor site passively. Studies have shown that the tumor accumulation of both targeted and non-targeted liposomes, as well as other DDS with a diameter exceeding 10 nm, did not markedly changed with active targeting.[16,26] It has been previously reported that tumor accumulation may even decrease when the targeting ligand enhances DDS uptake by the liver and spleen, consequently reducing blood half-life—a critical factor for efficient EPR-based accumulation.[27] Therefore, in larger DDS (over the renal elimination threshold), active targeting can rather be expected to improve long term retention and cellular internalization.[16] However, whether this translates into enhanced therapeutic efficacy needs to be carefully proven.

Many biological ligands have been identified and studied for facilitating active targeting of DDS to tumor cells, such as proteins, small peptides (transferrin, RGD, bombesin, or NR7), antibodies, affibodies, antibody-guided avidin-nucleic-acid nanoassemblies (ANANAS), polysaccharides (HA), and small molecules (folate – vitamin B9).[11,28] Often these are directed to surface molecules that are specific for only one or few cancer types, which limits their broad applicability and thus, commercial potential. To efficiently target one of cancers' general hallmarks, we exploited riboflavin's (RF) pivotal role in metabolically active tissues, i.e., cancer cells.[29] RF is highly requested for the formation of FAD and FMN, two coenzymes involved in energy metabolism, cell respiration, antibody production, growth, and development.[30] While there have been compelling evidence demonstrating RF's ability to significantly enhance internalization of DDS such as liposomes,[26] dendrimers,[31] linear[32,33] and star-shaped polymers,[16,17] the effect on chemotherapies' therapeutic outcome still needed to be elucidated.

In this study, we successfully prepared RF-targeted 4-arm PEG stars

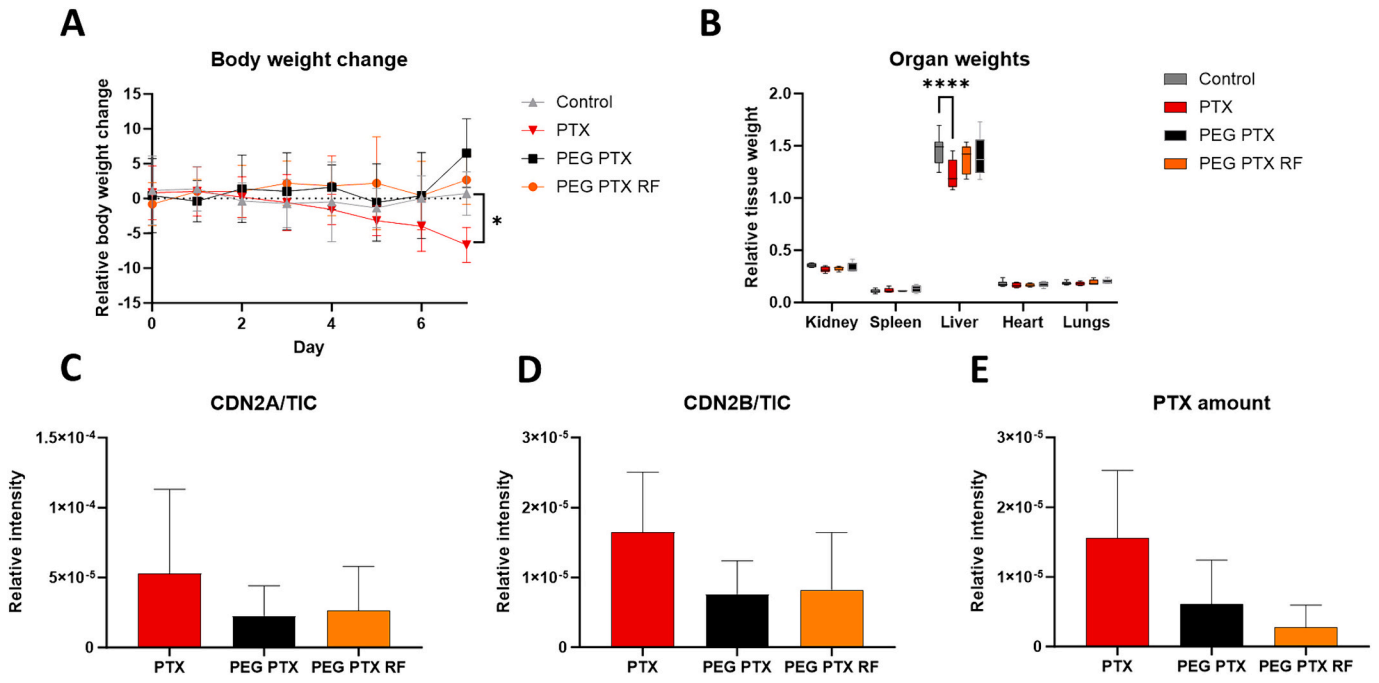

Fig. 7. Side effects of the treatment. The body weights of control, PEG PTX, and PEG PTX RF groups are comparable, while animals receiving free PTX have significantly lower values (A). Moreover, mice of this group have significantly lower liver weights (B) than control and PEG PTX or PEG PTX RF treated animals. Other organ weights are not affected by the therapy. Mass spectroscopy analysis confirmed these findings by showing that the free PTX treatment results in high values of mitosis inhibitor markers (C, D). Both PEG PTX and PEG PTX RF groups show relatively lower expressions of CDN2A and 2B. Furthermore, higher amounts of PTX metabolite (E) are found in livers that received free PTX than in the PEG PTX and PEG PTX RF groups indicating higher off-site accumulation and metabolization of the chemotherapeutic agent. *: $p \leq 0.05$.

conjugated with PTX (referred to as PEG PTX RF). Based on our previous experience with 4-arm PEG stars, sizes similar to those of immunoglobulins (5–15 nm) were expected.[16] However, we observed that larger sizes. In the previous study, the polymers were labeled with a fluorescent probe in order to detect them in vivo, while in our case, PEG stars were not labeled. Instead, they were conjugated to a chemotherapeutic drug to test therapeutic efficacy of actively targeting RF. Upon conjugation to PTX, the polymers tended to form supramolecular structures. Since these clusters are only held together via hydrophobic interactions, it is expected that the polymers can adapt and change formation. This was evaluated using molecular dynamic simulations. While the notion of supramolecular structure formation was also seen during dynamic simulations, it was also observed that RF had freedom to move. Additionally, an interaction of RF targeted polymers with BSA was observed highlighting the potential for RF to interact effectively with its surroundings, a crucial aspect of active targeting. The findings were further confirmed by the in vitro RBP binding assay, providing clear evidence that PEG PTX RF can bind to its intended targets.

As evidenced by our in vitro data, we observed that RF targeting of PEG PTX improves cytotoxicity on A431 and PC3 cells, which is in line with previous findings.[31,34–38] However, in comparison to the free drug, PEG PTX RF and PEG PTX showed lower efficacy, which is likely because drug delivery systems need more time to be internalized via endocytosis and to release the drug, while free PTX can quickly be transported into the cells via passive diffusion. Similar in vitro results with free drugs having higher efficacy than RF conjugates were obtained by others.[32,39,40]

In vivo, all treatments yielded similar tumor responses in terms of tumor size reduction, vascularization, and perfusion. As observed by Bartlett et al., the in vivo biodistribution and organ distribution of DDS changed only slightly following the conjugation of ligands.[41] Nevertheless, the ligands significantly enhanced the binding and uptake of DDS after reaching the tumor tissue. This may lead to prolonged therapy effects, which is indicated by our finding that tumors of animals treated with PEG PTX RF presented with the lowest amount of proliferating cells. Hence, further studies should be conducted to explore tumor progression after the end of treatment and investigate the effect of different treatment regimens in additional tumor models. Other strategies to enhance DDS therapeutic efficacy involve modifying the physicochemical properties of DDS, including size (different length of PEG chains), shape (linear or dendritic instead of star) rigidity, or surface properties. For instance, a study demonstrated that linear PEG PTX with a 20 kDa size exhibited higher in vitro toxicity than the 6 kDa compound.[42] Consistent with our initial hypothesis, we observed more side effects (loss of liver and body weight) in animals treated with free PTX compared to those receiving targeted and non-targeted DDS. Although PTX is known to be hepatotoxic, ex vivo histological examination of the livers (data not shown) did not reveal any significant differences between the control, free PTX, PEG-PTX, and RF-PEG-PTX groups. It is known that the acute toxicity of chemotherapeutics is often reflected by round lipid vacuoles indicating lipidosis or hepatic steatosis.[43] However, this effect is very transient due to the high regenerative capacity of the liver.[44] As we sacrificed our animals three days after the last drug administration, the acute effects of free PTX were most likely already gone. Therefore, we investigated the livers via mass spectrometry (MS), which highlighted the increased expression of cyclin-dependent kinase (CDNs) inhibitors and the prominent presence of PTX's main metabolite only in animals treated with free PTX. CDN2A and 2B are crucial regulatory proteins involved in cell cycle control and cell growth regulation. They inhibit the activity of cyclin-dependent kinases and arrest the cell cycle between G1 and S phase. The combined effect of the latter, along with the cytotoxicity provided by free PTX, exemplifies the lower liver weight of animals belonging to the group treated with free PTX. These findings underscore the significant advantage in employing DDS to reduce off-target toxicity, as previously demonstrated also with Doxil. The reduced side effects by using DDS would also justify the administration of higher PTX dosages to further enhance therapeutic efficacy.[34,35] Thus, dose escalation experiments with PEG PTX, and RF PEG

PTX will be a focus of our next studies.

In summary, this study's findings show that drug delivery systems are effective in reducing off-target accumulation of drugs. In addition, RF can enhance the cellular internalization of DDS, which accumulation potentially improves their long-term therapeutic efficacy.

Ethics approval

All animal experiments were approved by the governmental authority for animal care (in North Rhine Westfalia the Landesamt für Natur, Umwelt und Verbraucherschutz Nordrhein-Westfalen (LANUV)).

Funding

This research was supported by the Deutsche Forschungsgemeinschaft (DFG) in the framework of the Research Training Group 2375 "Tumor-targeted Drug Delivery" grant 331065168, the German Research Foundation in the Package Proposals PAK 961 (DFG – Project number: 403039938), DFG FOR 2591 to F.K. (grant 321137804), DFG Project-ID 445703531 and by the Transregional Collaborative Research Centre (TRR 219; Project-ID 322900939) to J.J. (subproject S-03 and C-04) and J.H. (subproject S-03, INST 948/4S-1 FU6.6), the START-Program of the Faculty of Medicine of the RWTH Aachen University, and by a grant from the Interdisciplinary Centre for Clinical Research within the faculty of Medicine at the RWTH Aachen University (PTD 1-1). Additionally, M.D. was supported by Cancer Research Center Cologne Essen (CCCE).

CRediT authorship contribution statement

Milita Darguzyte: Conceptualization, Investigation, Visualization, Writing – original draft, Writing – review & editing. **Elena Rama:** Investigation, Writing – original draft, Writing – review & editing. **Anne Rix:** Investigation, Writing – review & editing. **Jasmin Baier:** Investigation. **Juliane Hermann:** Investigation. **Sima Rezvantalab:** Investigation. **Mohammad Khedri:** Investigation. **Joachim Jankowski:** Supervision, Funding acquisition, Investigation. **Fabian Kiessling:** Conceptualization, Funding acquisition, Resources, Supervision.

Declaration of competing interest

The authors declare that they have no known competing financial interests or personal relationships that could have appeared to influence the work reported in this paper.

Acknowledgements

Marek Weiler for performing NTA measurements and helping with HPLC. Se-Hyeong Jung for help with multi-angle DLS measurements.

Appendix A. Supplementary data

Supplementary data to this article can be found online at https://doi.org/10.1016/j.nano.2024.102751.

References

1. Bonnet S. Why develop photoactivated chemotherapy? *Dalton Trans*. 2018;47(31):10330–10343.
2. Yan L, Shen J, Wang J, Yang X, Dong S, Lu S. Nanoparticle-based drug delivery system: a patient-friendly chemotherapy for oncology. *Dose-Response*. 2020 Jul 1;18(3), 1559325820936161.
3. Germain M, Caputo F, Metcalfe S, Tosi G, Spring K, Åslund AKO, et al. Delivering the power of nanomedicine to patients today. *J Control Release*. 2020 Oct 10;(326):164–171.
4. Sun R, Xiang J, Zhou Q, Piao Y, Tang J, Shao S, et al. The tumor EPR effect for cancer drug delivery: current status, limitations, and alternatives. *Adv Drug Deliv Rev*. 2022 Dec 1;191, 114614.
5. Matsumura Y, Maeda H. A new concept for macromolecular therapeutics in Cancer chemotherapy: mechanism of Tumoritropic accumulation of proteins and the antitumor agent Smancs1. *Cancer Res*. 1986 Dec 1;46(12_Part_1), 6387–92.
6. Dasgupta A, Biancacci I, Kiessling F, Lammers T. Imaging-assisted anticancer nanotherapy. *Theranostics*. 2020 Jan 1;10(3):956–967.
7. Ojha T, Pathak V, Shi Y, Hennink WE, Moonen CTW, Storm G, et al. Pharmacological and physical vessel modulation strategies to improve EPR-mediated drug targeting to tumors. *Adv Drug Deliv Rev*. 2017 Sep 15;119:44–60.
8. Shi J, Kantoff PW, Wooster R, Farokhzad OC. Cancer nanomedicine: progress, challenges and opportunities. *Nat Rev Cancer*. 2017 Jan;17(1):20–37.
9. Storm TL, Kiessling Fabian, Hennink Wim E, Gert. *Drug targeting to tumors: principles, pitfalls and (pre-) clinical progress. in: nano-enabled medical applications*. Jenny Stanford Publishing; 2020.
10. Pearce AK, O'Reilly RK. Insights into active targeting of nanoparticles in drug delivery: advances in clinical studies and design considerations for cancer nanomedicine. *Bioconjug Chem*. 2019 Sep 18;30(9):2300–2311.
11. Yoo J, Park C, Yi G, Lee D, Koo H. Active targeting strategies using biological ligands for nanoparticle drug delivery systems. *Cancers*. 2019 May;11(5):640.
12. Salahpour Anarjan F. Active targeting drug delivery nanocarriers: ligands. *Nano-Struct Nano-Obj*. 2019 Jul 1;19, 100370.
13. Taiariol L, Chaix C, Farre C, Moreau E. Click and bioorthogonal chemistry: the future of active targeting of nanoparticles for nanomedicines? *Chem Rev*. 2022 Jan 12;122(1):340–384.
14. Beztsinna N, Solé M, Taib N, Bestel I. Bioengineered riboflavin in nanotechnology. *Biomaterials*. 2016 Feb 1;80:121–133.
15. Bartmann L, Schumacher D, von Stillfried S, Sternkopf M, Alampour-Rajabi S, van Zandvoort MAMJ, et al. Evaluation of riboflavin transporters as targets for drug delivery and theranostics. *Front Pharmacol*. 2019;[cited 2023 Sep 5];10. https://doi.org/10.3389/fphar.2019.00079. Available from:.
16. Tsvetkova Y, Beztsinna N, Baues M, Klein D, Rix A, Golombek SK, et al. Balancing passive and active targeting to different tumor compartments using riboflavin-functionalized polymeric nanocarriers. *Nano Lett*. 2017 Aug 9;17(8):4665–4674.
17. Darguzyte M, Holm R, Baier J, Drude N, Schultze J, Koynov K, et al. Influence of riboflavin targeting on tumor accumulation and internalization of Peptostar based drug delivery systems. *Bioconjug Chem*. 2020 Dec 16;31(12):2691–2696.
18. Hoo CM, Starostin N, West P, Mecartney ML. A comparison of atomic force microscopy (AFM) and dynamic light scattering (DLS) methods to characterize nanoparticle size distributions. *J Nanopart Res*. 2008 Dec 1;10(1):89–96.
19. Jamting ÅK, Cullen J, Coleman VA, Lawn M, Herrmann J, Miles J, et al. Systematic study of bimodal suspensions of latex nanoparticles using dynamic light scattering. *Adv Powder Technol*. 2011 Mar;22(2):290–293.
20.. FDA Approved PEGylated Drugs By 2023 [Internet] [cited 2023 Sep 5]. Available from: https://www.biochempeg.com/article/58.html.
21. Johnson T, Ouhtit A, Gaur R, Fernando A, Schwarzenberger P, Su J, et al. Biochemical characterization of riboflavin carrier protein (RCP) in prostate cancer. *Front Biosci (Landmark Ed)*. 2009 Jan 1;14(10):3634–3640.
22. Lee C, Jeong H, Lee KH, Park S, Gang MJ, Bae SK, et al. Evaluation of the efficacy and safety of the herbal formula PM014 in a cisplatin- and paclitaxel-treated tumor-bearing mouse model. *Integr Cancer Ther*. 2020 Jun 26;19, 1534735420924711.
23. Zhao X, Fan J, Wu P, Wei C, Chen Q, Ming Z, et al. Chronic chemotherapy with paclitaxel nanoparticles induced apoptosis in lung cancer in vitro and in vivo. *Int J Nanomedicine*. 2019 Feb 19;14:1299–1309.
24. Xia Y, Rao L, Yao H, Wang Z, Ning P, Chen X. Engineering macrophages for cancer immunotherapy and drug delivery. *Adv Mater*. 2020;32(40), 2002054.
25. Dutta B, Barick KC, Hassan PA. Recent advances in active targeting of nanomaterials for anticancer drug delivery. *Adv Colloid Interf Sci*. 2021 Oct 1;296, 102509.
26. Beztsinna N, Tsvetkova Y, Bartneck M, Lammers T, Kiessling F, Bestel I. Amphiphilic phospholipid-based riboflavin derivatives for tumor targeting nanomedicines. *Bioconjug Chem*. 2016 Sep 21;27(9):2048–2061.
27. Kunjachan S, Pola R, Gremse F, Theek B, Ehling J, Moeckel D, et al. Passive versus active tumor targeting using RGD- and NGR-modified polymeric nanomedicines. *Nano Lett*. 2014 Feb 12;14(2):972–981.
28. Muhamad N, Plengsuriyakarn T, Na-Bangchang K. Application of active targeting nanoparticle delivery system for chemotherapeutic drugs and traditional/herbal medicines in cancer therapy: a systematic review. *Int J Nanomedicine*. 2018 Jul 4;13:3921–3935.
29. Hanahan D. Hallmarks of cancer: new dimensions. *Cancer Discov*. 2022 Jan;12(1):31–46.
30. Balasubramaniam S, Christodoulou J, Rahman S. Disorders of riboflavin metabolism. *J Inherit Metab Dis*. 2019;42(4):608–619.
31. Thomas TP, Choi SK, Li MH, Kotlyar A, Baker JR. Design of riboflavin-presenting PAMAM dendrimers as a new nanoplatform for cancer-targeted delivery. *Bioorg Med Chem Lett*. 2010 Sep 1;20(17):5191–5194.
32. Mu J, Zhong H, Zou H, Liu T, Yu N, Zhang X, et al. Acid-sensitive PEGylated paclitaxel prodrug nanoparticles for cancer therapy: effect of PEG length on antitumor efficacy. *J Control Release*. 2020 Oct 10;326:265–275.
33. Bareford LM, Avaritt BR, Ghandehari H, Nan A, Swaan PW. Riboflavin-targeted polymer conjugates for breast tumor delivery. *Pharm Res*. 2013 Jul 1;30(7):1799–1812.
34. Waterhouse DN, Tardi PG, Mayer LD, Bally MB. A comparison of liposomal formulations of doxorubicin with drug administered in free form. *Drug-Safety*. 2001 Oct 1;24(12):903–920.
35. Rafiyath SM, Rasul M, Lee B, Wei G, Lamba G, Liu D. Comparison of safety and toxicity of liposomal doxorubicin vs conventional anthracyclines: a meta-analysis. *Exp Hematol Oncol*. 2012 Apr 23;1:10.

36. Cavallaro G, Licciardi M, Caliceti P, Salmaso S, Giammona G. Synthesis, physico-chemical and biological characterization of a paclitaxel macromolecular prodrug. *Eur J Pharm Biopharm*. 2004 Jul 1;58(1):151–159.
37. Deutsch HM, Glinski JA, Hernandez M, Haugwitz RD, Narayanan VL, Suffness M, et al. Synthesis of congeners and prodrugs. 3. Water-soluble prodrugs of taxol with potent antitumor activity. *J Med Chem*. 1989 Apr;32(4):788–792.
38. Caelen I, Kalman A, Wahlström L. Biosensor-based determination of riboflavin in Milk samples. *Anal Chem*. 2004 Jan 1;76(1):137–143.
39. Bareford LM, Avaritt BR, Ghandehari H, Nan A, Swaan PW. Riboflavin-targeted polymer conjugates for breast tumor delivery. *Pharm Res*. 2013 Jul 1;30(7):1799–1812.
40. Thomas TP, Choi SK, Li MH, Kotlyar A, Baker JR. Design of riboflavin-presenting PAMAM dendrimers as a new nanoplatform for cancer-targeted delivery. *Bioorg Med Chem Lett*. 2010 Sep 1;20(17):5191–5194.
41. Bartlett DW, Su H, Hildebrandt IJ, Weber WA, Davis ME. Impact of tumor-specific targeting on the biodistribution and efficacy of siRNA nanoparticles measured by multimodality in vivo imaging. *Proc Natl Acad Sci U S A*. 2007 Sep 25;104(39):15549–15554.
42. Luo T, Magnusson J, Préat V, Frédérick R, Alexander C, Bosquillon C, et al. Synthesis and in vitro evaluation of polyethylene glycol-paclitaxel conjugates for lung cancer therapy. *Pharm Res*. 2016 Jul 1;33(7):1671–1681.
43. Josan S, Billingsley K, Orduna J, Park JM, Luong R, Yu L, et al. Assessing inflammatory liver injury in an acute CCl4 model using dynamic 3D metabolic imaging of hyperpolarized [1-13C]pyruvate. *NMR Biomed*. 2015;28(12):1671–1677.
44. Michalopoulos GK, Bhushan B. Liver regeneration: biological and pathological mechanisms and implications. *Nat Rev Gastroenterol Hepatol*. 2021 Jan;18(1):40–55.